Fuzzy Exponential Recurrent Neural Networks for Gray-scale Image Retrieval*

Marcos Eduardo Valle

University of Campinas, Department of Applied Mathematics,
CEP 13083-859. Campinas – SP, Brazil
E-mail: valle@ime.unicamp.br

Abstract. Associative memories (AMs) are mathematical models inspired by the human brain ability to store and recall information. This paper introduces the fuzzy exponential recurrent neural networks (FERNNs), which can implement an AM for the storage and recall of fuzzy sets. The novel models are obtained by modifying the multivalued exponential recurrent neural network of Chiueh and Tsai. Briefly, a FERNN defines recursively a sequence of fuzzy sets obtained by averaging the stored fuzzy sets weighted by an exponential of a fuzzy comparison measure between the current fuzzy set and the stored items. Computational experiments reveal that FERNNs can be effectively used for the retrieval of gray-scale images corrupted by either Gaussian noise or salt-and-pepper noise.

Keywords: Associative memory, recurrent neural network, fuzzy system, gray-scale image processing.

1 Introduction

Associative memories (AMs) are mathematical constructs motivated by the human brain ability to store and recall information [1]. Such as the biological neural network, an AM should be able to retrieve a memorized information from a possibly incomplete or corrupted item. Formally, an AM is designed for the storage of a finite set $\{\mathbf{a}^1, \mathbf{a}^2, \ldots, \mathbf{a}^p\}$, called the *fundamental memory set*. Afterwards, the AM model is expect to retrieve a memorized concept $\mathbf{a}^\xi$ in response to the presentation of a partial or noisy version $\tilde{\mathbf{a}}^\xi$ of $\mathbf{a}^\xi$. Applications of AMs cover, for instance, pattern classification and recognition [2–4], optimization [5], computer vision and image retrieval [6–8], prediction [9, 10], control [11, 12], and language understanding [13].

The *Hopfield neural network* is one of the most widely known neural network used to realize an AM [14]. In spite of its attractive features, including a characterization in terms of an energy function and a variety of applications [15], the Hopfield network suffers from a low absolute storage capacity. Specifically, the asymptotic number of items that can be stored and subsequently recovered exactly by the Hopfield network is proportional to $n/log(n)$, where n is the length of the vectors $\mathbf{a}^\xi$, for $\xi = 1, \ldots, p$ [16]. A simple but significant improvement in storage capacity of the Hopfield network is

* This work was supported in part by by CNPq under grant no. 304240/2011-7, FAPESP under grant no. 2013/12310-4, and FAEPEX/Unicamp under grant no. 519.292.

achieved by the *recurrent correlation neural networks* (RCNNs) introduced by Chiueh and Goodman in the early 1990s [17]. In few words, Chiueh and Goodman generalized the Hopfield network by adding a layer of nodes that compute a correlation measure between the current state and the fundamental memories. The activation function of the neurons in this layer characterizes the RCNN. For example, an *exponential recurrent correlation neural network* (exponential RCNN) is obtained by considering an exponential function. The storage capacity of some RCNNs, including the exponential RCNNs, scales exponentially with the length of the vectors [17]. Besides the very high storage capacity, these neural networks exhibit excellent error correction capabilities. On the downside, such as the Hopfield network, the original RCNNs are designed for the storage and recall of bipolar vectors. However, many applications of AMs, including the retrieval of gray-scale images in the presence of noise, require the storage and recall of real-valued vectors or fuzzy sets [2–4, 6–12].

In 1993, Chiueh and Tsai extended the bipolar exponential RCNNs for the storage and recall of multivalued vectors [18]. The major components of the novel model include a weighted average and a kind of similarity measure. Now, since a weighted average performs an aggregation of fuzzy sets [19] and, considering some well established fuzzy similarity measures, in this paper we modified the multivalued exponential RCNNs for the storage and recall of fuzzy sets in a rather straightforward manner. The novel models, referred to as *fuzzy exponential recurrent neural networks* (FERNNs), outperformed many other AM models from the literature, including two multivalued exponential RCNNs, in a computational experiment concerning the retrieval of gray-scale images corrupted by either Gaussian noise or salt-and-pepper noise.

The paper is organized as follows: Section 2 briefly reviews the multivalued exponential recurrent neural network of Chiueh and Tsai. The novel FERNNs are introduced in Section 3. Computational experiments concerning the retrieval of corrupted gray-scale images are given in Section 4. The paper finishes with some concluding remarks in Section 5.

2 Multivalued Exponential Recurrent Neural Network

The *multivalued exponential recurrent neural networks* (MERNNs) are able to implement hight-capacity AMs with excellent noise tolerance. These models, introduced by Chiueh and Tsai in the early 1990s, are obtained by extending the exponential recurrent correlation neural network for the storage and recall of multi-valued vectors according to [17, 18]. Formally, a MERNN is designed as follows.

Let $\mathbb{K} = \{\kappa_1, \kappa_2, \ldots, \kappa_K\}$ denote a K-valued set and α be a positive real number. Also, consider a fundamental memory set $\{\mathbf{a}^1, \ldots, \mathbf{a}^p\} \subseteq \mathbb{K}^n$, where each $\mathbf{a}^\xi$ is a multivalued column vector. Given a multivalued input vector $\mathbf{x}_0 \in \mathbb{K}^n$, the MERNN defines recursively the sequence of vectors $\mathbf{x}_0, \mathbf{x}_1, \ldots$ according to the equation

$$\mathbf{x}_{t+1} = \frac{\sum_{\xi=1}^{p} \mathbf{a}^\xi e^{\alpha \Psi\left(\mathbf{a}^\xi, \mathbf{x}_t\right)}}{\sum_{\xi=1}^{p} e^{\alpha \Psi\left(\mathbf{a}^\xi, \mathbf{x}_t\right)}}, \quad \forall t = 0, 1, \ldots, \tag{1}$$

where $\Psi\left(\mathbf{a}^\xi, \mathbf{x}_t\right)$ measures – in a broad sense – the similarity between $\mathbf{a}^\xi$ and $\mathbf{x}_t$. For example, Ψ may refer to the direction cosine or the Euclidean distance-based similarity measure given respectively by

$$\Psi_C(\mathbf{a}^\xi, \mathbf{x}_t) = \frac{\langle \mathbf{a}^\xi, \mathbf{x}_t \rangle}{\|\mathbf{a}^\xi\|_2 \|\mathbf{x}_t\|_2} \quad \text{and} \quad \Psi_E(\mathbf{a}^\xi, \mathbf{x}_t) = \frac{1}{1 + \|\mathbf{a}^\xi - \mathbf{x}_t\|_2}, \tag{2}$$

where $\langle \cdot, \cdot \rangle$ denotes the usual inner product and $\| \cdot \|_2$ is the Euclidean norm.

Alternatively, the vector $\mathbf{x}_{t+1}$ produced by the MERNN can be expressed as the weighted average

$$\mathbf{x}_{t+1} = \sum_{\xi=1}^{p} w_{t\xi} \mathbf{a}^\xi, \tag{3}$$

where the dynamic weight $w_{t\xi}$ is computed by

$$w_{t\xi} = \frac{e^{\alpha \Psi\left(\mathbf{a}^\xi, \mathbf{x}_t\right)}}{\sum_{\xi=1}^{p} e^{\alpha \Psi\left(\mathbf{a}^\xi, \mathbf{x}_t\right)}}, \quad \forall \xi = 1, \ldots, p \quad \text{and} \quad t = 0, 1, \ldots \tag{4}$$

3 Fuzzy Exponential Recurrent Neural Network

The MERNNs can be modified in a rather straightforward manner for the storage and recall of fuzzy sets. Precisely, let $\alpha > 0$ be a real number and consider a fundamental memory set $\{\mathbf{a}^1, \mathbf{a}^2, \ldots, \mathbf{a}^p\} \subseteq \mathcal{F}(U)$, where each $\mathbf{a}^\xi$ is a fuzzy set in U. Given an input fuzzy set $\mathbf{x}_0 \in \mathcal{F}(U)$, a *fuzzy exponential recurrent neural network* (FERNN) defines the sequence $\mathbf{x}_1, \mathbf{x}_2, \ldots$ of fuzzy sets in U by means of the equation

$$\mathbf{x}_{t+1}(u) = \sum_{\xi=1}^{p} w_{t\xi} \mathbf{a}^\xi(u), \quad \forall u \in U \quad \text{and} \quad t = 0, 1, \ldots \tag{5}$$

where the weights are computed as follows for all $\xi = 1, \ldots, p$ and $t \geq 0$:

$$w_{t\xi} = \frac{e^{\alpha \Upsilon(\mathbf{a}^\xi, \mathbf{x}_t)}}{\sum_{\xi=1}^{p} e^{\alpha \Upsilon(\mathbf{a}^\xi, \mathbf{x}_t)}}, \tag{6}$$

and $\Upsilon(\mathbf{a}^\xi, \mathbf{x}_t)$ denotes a fuzzy comparison measure, such as a similarity or an overlapping measure [19], between the fuzzy sets $\mathbf{a}^\xi$ and $\mathbf{x}_t$. For simplicity, in the following we only consider Υ equals to a similarity measure $\mathcal{S}$. Recall that similarity measures have a broad range of applications including, for instance, fuzzy neural networks [3], fuzzy clustering [20], linguistic approximation [21], and fuzzy reasoning [22].

Broadly speaking, a similarity measure $\mathcal{S}(\mathbf{a}^\xi, \mathbf{x}_t)$ indicates the degree to which the fuzzy sets $\mathbf{a}^\xi$ and $\mathbf{x}_t$ are equal. Formally, a similarity measure is a function $\mathcal{S} : \mathcal{F}(U) \times \mathcal{F}(U) \to [0, 1]$ that satisfies the following four properties for any fuzzy sets $\mathbf{a}, \mathbf{b}, \mathbf{c} \in \mathcal{F}(U)$:

1. $\mathcal{S}(\mathbf{a}, \mathbf{b}) = \mathcal{S}(\mathbf{b}, \mathbf{a})$.

2. $\mathcal{S}(A, A^c) = 0$ for all crisp set $A \in \mathcal{P}(U)$.
3. $\mathcal{S}(\mathbf{a}, \mathbf{a}) = 1$.
4. If $\mathbf{a} \subseteq \mathbf{b} \subseteq \mathbf{c}$, then $\mathcal{S}(\mathbf{a}, \mathbf{c}) \leq \mathcal{S}(\mathbf{a}, \mathbf{b})$ and $\mathcal{S}(\mathbf{a}, \mathbf{c}) \leq \mathcal{S}(\mathbf{b}, \mathbf{c})$.

We would like to point out that the preceding definition corresponds to a normalized version of the axiomatic definition given by Xuecheng [23]. Some researchers, such as Li [24] and Zeng [25], replace condition 2 by $\mathcal{S}(U, \emptyset) = 0$. Also, condition 3 is sometimes substituted by the equivalence $\mathcal{S}(\mathbf{a}, \mathbf{b}) = 1 \iff \mathbf{a} = \mathbf{b}$.

Examples of similarity measure between two fuzzy sets $\mathbf{a}, \mathbf{b} \in \mathcal{F}(U)$ defined on a finite universe of discourse $U = \{u_1, \ldots, u_n\}$ include [21, 26]:

1. Gregson similarity measure:

$$\mathcal{S}_G(\mathbf{a}, \mathbf{b}) = \frac{\sum_{j=1}^{n} (\mathbf{a}(u_j) \wedge \mathbf{b}(u_j))}{\sum_{j=1}^{n} (\mathbf{a}(u_j) \vee \mathbf{b}(u_j))}, \tag{7}$$

   where the symbols "$\vee$" and "$\wedge$" denotes respectively to the maximum and minimum operations.
2. Eisler and Ekman similarity measure:

$$\mathcal{S}_E(\mathbf{a}, \mathbf{b}) = \frac{2\sum_{j=1}^{n} (\mathbf{a}(u_j) \wedge \mathbf{b}(u_j))}{\sum_{j=1}^{n} \mathbf{a}(u_j) + \sum_{j=1}^{n} \mathbf{b}(u_j)}. \tag{8}$$

3. Relative Hamming distance:

$$\mathcal{S}_H(\mathbf{a}, \mathbf{b}) = 1 - \frac{1}{n} \sum_{j=1}^{n} |\mathbf{a}(u_j) - \mathbf{b}(u_j)|. \tag{9}$$

We would like to point out that there are many other similarity measures available at the literature. For simplicity, however, we consider in this paper only the three functions given above. We plan to further investigate fuzzy comparison measures and their effects on FERNNs in the future.

4 Computational Experiments

Let us perform some experiments concerning the retrieval of corrupted gray-scale images. Specifically, consider the eight gray-scale images that are displayed in Figure 1. These images have size 128×128 and 256 gray levels. For each of these images, we generated a column-vector $\mathbf{a}^\xi \in [0, 1]^n$, $\xi = 1, \ldots, 8$ and $n = 16384$, using the standard row-scan method and dividing the 8-bit intensities by 255. Note that $\mathbf{a}^\xi = [a_1^\xi, \ldots, a_n^\xi]^T$ can be interpreted as a fuzzy set on a finite universe of discourse $U = \{u_1, \ldots, u_n\}$, that is, the component a_j^ξ corresponds to the degree to which the element u_j belongs to the fuzzy set $\mathbf{a}^\xi$, for any $j = 1, \ldots, n$. Therefore, the eight gray-scale images can be stored in the FERNNs obtained by considering the similarity measures $\mathcal{S}_G$, $\mathcal{S}_E$, and $\mathcal{S}_H$. The eight gray-scale images can also be stored in the two MERNNs obtained by considering the multivalued set $\mathbb{K} = \{0, 1/255, \ldots, 254/255, 1\}$ and the measures Ψ_C

Fig. 1. Original gray-scale images of size 128×128 and 256 gray-levels.

Table 1. PSNR rates produced by single-step MERNN and FERNN models upon presentation of the original images $\mathbf{a}^1, \ldots, \mathbf{a}^8$.

	$\mathbf{a}^1$	$\mathbf{a}^2$	$\mathbf{a}^3$	$\mathbf{a}^4$	$\mathbf{a}^5$	$\mathbf{a}^6$	$\mathbf{a}^7$	$\mathbf{a}^8$
MERNN Ψ_C	23.29	24.47	18.00	36.89	25.45	23.03	22.95	28.04
MERNN Ψ_E	166.30	165.61	163.02	163.50	165.37	166.48	165.65	164.78
FERNN $\mathcal{S}_H$	38.25	38.60	44.48	43.43	39.42	38.54	38.87	40.77
FERNN $\mathcal{S}_E$	39.27	40.66	37.36	58.40	48.62	39.00	37.75	46.38
FERNN $\mathcal{S}_G$	63.47	65.49	61.29	87.86	76.28	63.04	61.25	73.66

and Ψ_E given by (2). In the following experiments, we adopted $\alpha = 20$ in both FERNN and MERNN models.

First, we presented the original images $\mathbf{a}^1, \ldots, \mathbf{a}^8$ as inputs to the three FERNN as well as the two MERNNs. The *peak signal-to-noise ratio* (PSNR) rates produced by a single-step memory model is given in Table 1. In this paper, we computed the PSNR between vectors $\mathbf{x} \in [0,1]^n$ and $\mathbf{y} \in [0,1]^n$ by means of the equation

$$\text{PSNR} = 20 \log \left(\frac{\sqrt{n}}{\epsilon_{mach} \vee \|\mathbf{x} - \mathbf{y}\|_2} \right), \tag{10}$$

where ϵ_{mach}, introduced to avoid a division by zero, denotes the machine precision. In our case, ϵ_{mach} is approximately 2.22×10^{-16}. Hence, the upper bound for PSNR is approximately 355.22. Note that the MERNN Ψ_E outperformed the other networks. The second largest PSNR rates have been produced by the FERNN $\mathcal{S}_G$. The FERNNs based on the similarity measures $\mathcal{S}_H$ and $\mathcal{S}_E$ produced similar PSNR rates while the MERNN based on the direction cosine yielded the worst results. In spite of the difference in the PSNR rates, the single-step neural networks produced images visually similar to the original ones except for the MERNN Ψ_C. A visual interpretation of the output produced

Fig. 2. Images recovered by a single-step model upon presentation of the original image.

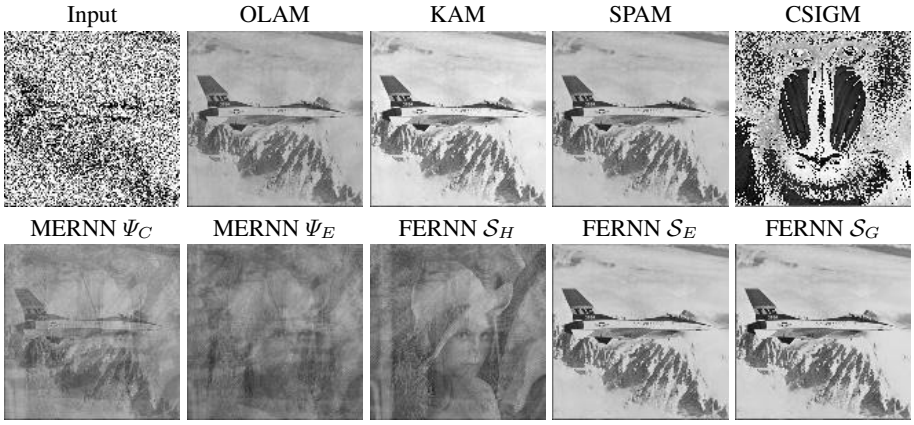

Fig. 3. Airplane image corrupted by Gaussian noise with variance 0.3 followed by the images retrieved by the memory models.

by the single-step recurrent networks upon presentation of the original image $\mathbf{a}^1$ is provided in Figure 2.

Let us now examine and compare the noise tolerance of the three novel FERNNs with the MERNN based on Ψ_C and Ψ_E. Specifically, we probed each neural network with gray-scale images corrupted by Gaussian noise with zero mean and variance ranging from 0 to 0.3. We also probed the recurrent neural networks with images corrupted by salt and pepper noise with densities varying from 0 to 0.8. Again, we considered the parameter $\alpha = 20$. Also, we iterated (3) and (5) either until $\|\mathbf{x}_{t+1} - \mathbf{x}_t\|_2 \leq 10^{-6}$ or $t < 20$. Figure 5 shows the average PSNR rates produced by the five recurrent networks averaged in 80 experiments, that is, each original image was distorted 10 times for a certain noise intensity. As remarked previously, the MERNN Ψ_E yielded the largest PSNR rates for undistorted images. Notwithstanding, the FERNN based on Gregson similarity measure $\mathcal{S}_G$ outperformed the other recurrent networks for patterns corrupted by either Gaussian noise or salt-and-pepper noise. In addition, the other two FERNN also produced average PSNR rates larger than the MERNNs based on Φ_E and Φ_C. In particular, the MERNN based on Φ_E is exceedingly sensitive to noise, that is, its error correction capability decreases considerably as the input patten is corrupted by either Gaussian or

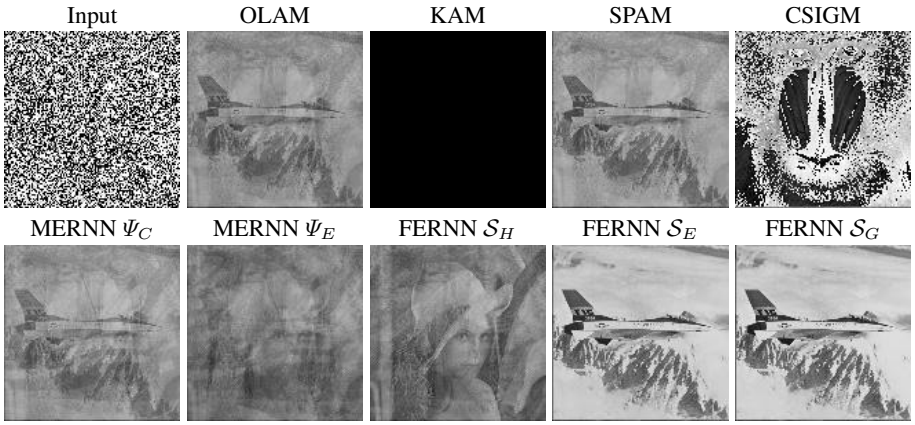

Fig. 4. Airplane image corrupted by salt-and-pepper noise with probability 0.8 followed by the images retrieved by the memory models.

Table 2. PSNR produced by the images in Figures 3 and 4.

	Input	OLAM	KAM	SPAM	CSIGM
Gaussian	8.78	20.12	24.21	26.13	7.00
Salt and Pepper	5.91	13.83	2.83	15.43	7.02
	MERNN Ψ_C	MERNN Ψ_E	FERNN $\mathcal{S}_H$	FERNN $\mathcal{S}_E$	FERNN $\mathcal{S}_G$
Gaussian	14.32	10.79	10.48	33.06	60.98
Salt and Pepper	14.32	10.79	10.48	33.11	60.98

salt-and-pepper noise. In contrast, the average PSNR rates produced by the FERNNs are greater than 30 even for highly corrupted input images. As the reader can see in the second row of Figures 3 and 4, the images retrieved by the FERNNs $\mathcal{S}_E$ and $\mathcal{S}_G$ upon presentation of the airplane image corrupted by either Gaussian noise with variance 0.3 or salt-and-pepper noise with probability 0.8 are visually similar to the original image. Table 2 contains the PSNR rates produced by the images shown in Figures 3 and 4. We would like to point out that the PSNR rates produced by the FERNNs $\mathcal{S}_G$ and $\mathcal{S}_E$ are higher in Table 2 than in Figure 5 because the recurrent network eventually converged to the wrong gray-scale image. For example, by feeding the FERNN based on Gregson similarity measure with the "lena" image corrupted by salt-and-pepper noise with probability 0.8 yielded as output the image "boat".

Finally, let us now examine and compare the noise tolerance of the FERNN $\mathcal{S}_G$ with other AM models for gray-scale patterns. Namely, let us confront the recurrent network based on Gregson similarity measure with the *optimal linear associative memory* (OLAM) [1], the *kernel associative memory* (KAM) [27], the *complex-sigmoid Hopfield network* (CSIGM) [28], and a certain *subspace projection autoassociative memory* (SPAM) [29]. Again, we probed the AM models with images corrupted by either Gaus-

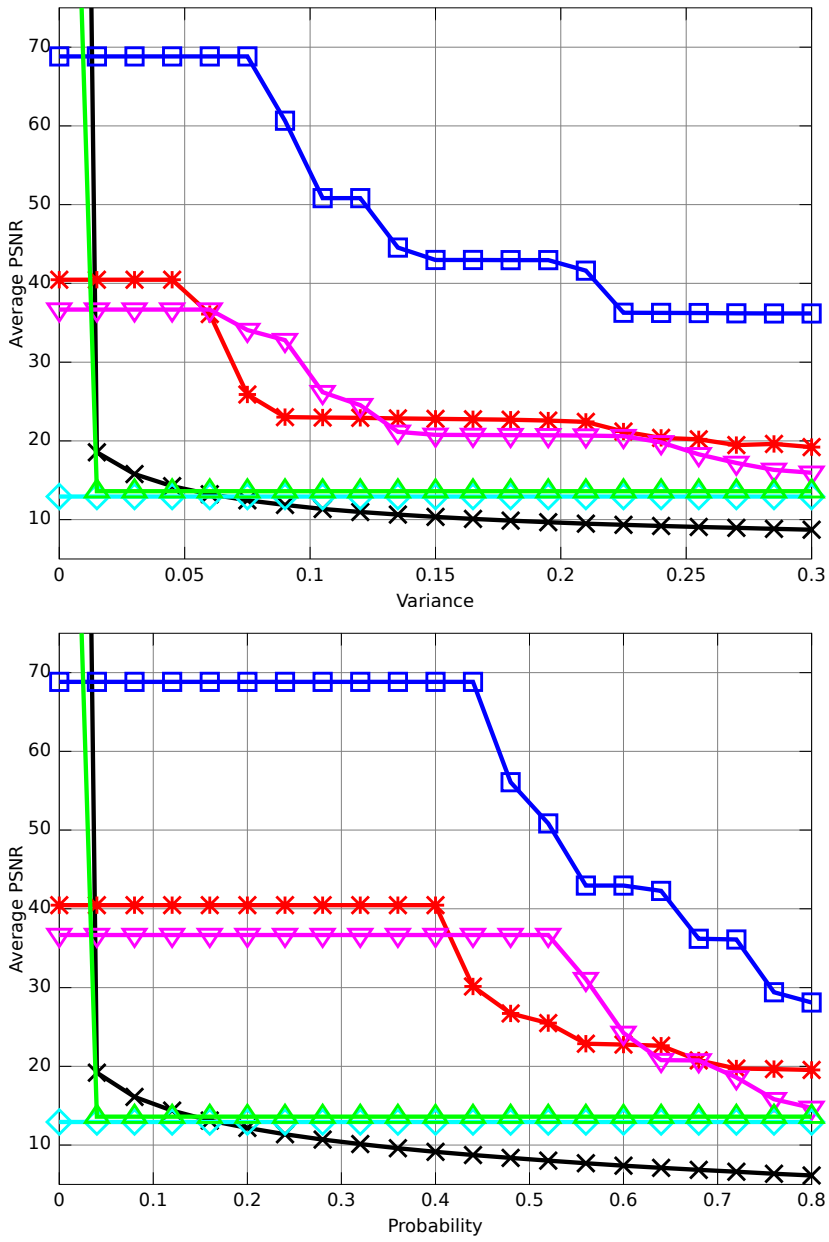

Fig. 5. Average PSNR versus the variance of the Gaussian noise (first row) or salt-and-pepper probability (second row). The line marked by "$\times$" represents the corrupted images. The lines marked by the symbols "$\square$", "$*$", "$\triangledown$", "$\triangle$", and "$\lozenge$" correspond respectively to the FERNNs $\mathcal{S}_G$, $\mathcal{S}_E$, and $\mathcal{S}_H$, and the MERNNs Ψ_E and Ψ_C.

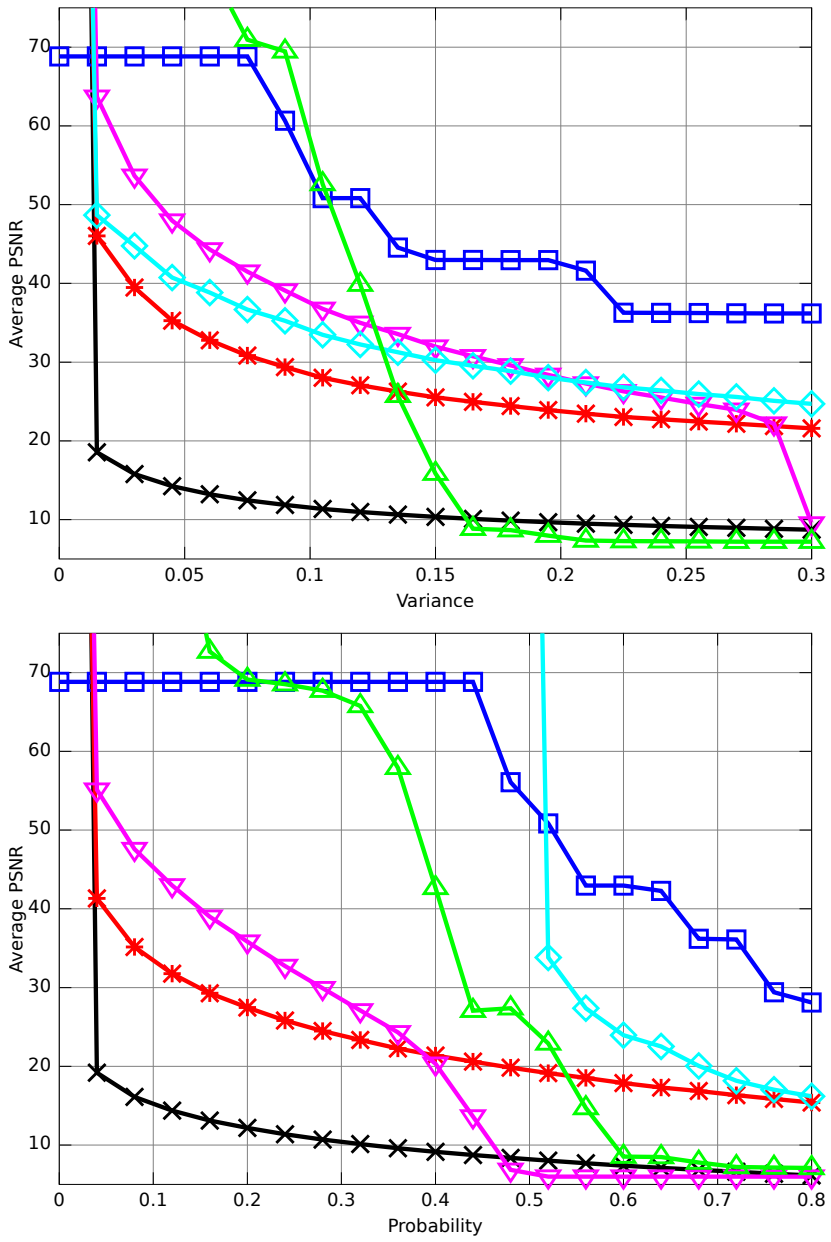

Fig. 6. Average PSNR versus Gaussian noise variance (first row) and the probability of salt-and-pepper noise (second row). The line marked by "×" represents the corrupted images. The lines marked by the symbols "□", "∗", "▽", "△", and "◊" correspond respectively to the FERNN $\mathcal{S}_G$, OLAM, and KAM, CSIGM, and SPAM.

sian noise and salt-and-pepper noise with different intensities. In analogy to Figure 5, Figure 6 plots the average PSNR rates by the noise intensity in 80 simulations. Figures 3 and 4 shows the image retrieved by all memory models for the "airplane" image corrupted by either Gaussian noise with variance 0.3 or salt-and-pepper noise with probability 0.8. Moreover, Table 2 contains the PSNR produced by the images depicted in Figures 3 and 4.

Note that the CSIGM model of Tanaka and Aihara produced the largest PSNR rates for images corrupted by Gaussian noise with variance less than 0.14. For larger variances, the novel FERNN based on Gregson similarity measure outperformed the other memory models. Similarly, the SPAM yielded the largest PSNR rates for images corrupted by salt-and-pepper noise with probability less than 0.52. Again, the FERNN $\mathcal{S}_G$ exhibited the best noise tolerance for gray-scale images corrupted by salt-and-pepper noise with probability greater than 0.52. Furthermore, by considering PSNR values greater than 40, in mean the FERNN $\mathcal{S}_G$ supports Gaussian noise and salt-and-pepper noise with intensities up to 0.22 and 0.64, respectively. At this point, note from Table 1 and 2 and Figures 2, 3, and 4 that two images are visually similar if PSNR ≥ 40. Thus, the novel FERNNs have potential applications for the retrieval of gray-scale images corrupted by either Gaussian noise or salt-and-pepper noise.

5 Concluding Remarks

In this paper, we introduced *fuzzy exponential recurrent neural networks* (FERNNs), which can be used for the storage and recall of fuzzy sets. A FERNN first compute a fuzzy comparison measure between the current fuzzy set with the fundamental fuzzy sets. The next fuzzy set is defined by the average of the fundamental fuzzy sets weighted by an exponential of the fuzzy comparison measure values. Computational experiments revealed that the novel FERNNs equipped with a similarity measure can be effectively used for the retrieval of corrupted gray-scale images.

In the future, we plant study the convergence of the sequence produced by an FERNN. We also intent to investigate the effect of the fuzzy comparison measure on the storage capacity as well as the noise tolerance of a FERNN used to implement an AM model. The relationship between the novel memories and other fuzzy AM models, including the bank of fuzzy associative memories of Kosko [11, 12] and the similarity measure fuzzy associative memory of Esmi and Sussner [3], require further attention. Finally, since an fuzzy associative memory can be used as a fuzzy inference engine [12], applications of the FERNN in rule-based systems can be explored in the future.

References

1. Kohonen, T.: Self-organization and associative memory. 2rd edition edn. Springer-Verlag New York, Inc., New York, NY, USA (1987)
2. Zhang, D., Zuo, W.: Computational Intelligence-Based Biometric Technologies. IEEE Computational Intelligence Magazine **2**(2) (May 2007) 26–36
3. Esmi, E.L., Sussner, P., Valle, M.E., Sakuray, F., Barros, L.: Fuzzy Associative Memories Based on Subsethood and Similarity Measures with Applications to Speaker Identification.

In: Lecture Notes in Computer Science: International Conference on Hybrid Artificial Intelligence Systems (HAIS 2012). Springer-Verlag Berlin Heidelberg, Berlin, Germany (2012) 479–490
4. Esmi, E.L., Sussner, P., Bustince, H., Fernández, J.: Θ-Fuzzy Associative Memories. IEEE Transactions on Fuzzy Systems Accepted for publication.
5. Hopfield, J., Tank, D.: Neural computation of decisions in optimization problems. Biological Cybernetics **52** (1985) 141–152
6. Sussner, P., Valle, M.E.: Grayscale Morphological Associative Memories. IEEE Transactions on Neural Networks **17**(3) (May 2006) 559–570
7. Urcid, G., Ritter, G.X., Valdiviezo-N., J.C.: Grayscale image recall from imperfect inputs with a two layer dendritic lattice associative memory. In: Proceedings of the Third World Congress on Nature & Biologically Inspired Computing (NaBIC 2011). (October 2011) 261–266
8. Sussner, P., Esmi, E.L., Villaverde, I., Graña, M.: The Kosko Subsethood Fuzzy Associative Memory (KS-FAM): Mathematical Background and Applications in Computer Vision. Journal of Mathematical Imaging and Vision **42**(2–3) (February 2012) 134–149
9. Sussner, P., Valle, M.E.: Recall of Patterns Using Morphological and Certain Fuzzy Morphological Associative Memories. In: Proceedings of the IEEE World Conference on Computational Intelligence 2006, Vancouver, Canada (2006) 209–216
10. Sussner, P., Miyasaki, R., Valle, M.E.: An Introduction to Parameterized IFAM Models with Applications in Prediction. In: Proceedings of the 2009 IFSA World Congress and 2009 EUSFLAT Conference, Lisbon, Portugal (July 2009) 247–252
11. Kong, S.G., Kosko, B.: Adaptive Fuzzy Systems for Backing up a Truck-and-Trailer. IEEE Transactions on Neural Networks **3**(2) (1992) 211–223
12. Kosko, B.: Neural Networks and Fuzzy Systems: A Dynamical Systems Approach to Machine Intelligence. Prentice Hall, Englewood Cliffs, NJ (1992)
13. Markert, H., Kaufmann, U., Kayikci, Z.K., Palm, G.: Neural associative memories for the integration of language, vision and action in an autonomous agent. Neural Networks **22**(2) (March 2009) 134–143
14. Hopfield, J.J.: Neural Networks and Physical Systems with Emergent Collective Computational Abilities. Proceedings of the National Academy of Sciences **79** (April 1982) 2554–2558
15. Hassoun, M.H.: Fundamentals of Artificial Neural Networks. MIT Press, Cambridge, MA (1995)
16. McEliece, R.J., Posner, E.C., Rodemich, E.R., Venkatesh, S.: The capacity of the Hopfield associative memory. IEEE Transactions on Information Theory **1** (1987) 33–45
17. Chiueh, T., Goodman, R.: Recurrent Correlation Associative Memories. IEEE Trans. on Neural Networks **2** (February 1991) 275–284
18. Chiueh, T.D., Tsai, H.K.: Multivalued associative memories based on recurrent networks. IEEE Transactions on Neural Networks **4**(2) (March 1993) 364–366
19. Pedrycz, W., Gomide, F.: Fuzzy Systems Engineering: Toward Human-Centric Computing. Wiley-IEEE Press, New York (2007)
20. Yager, R.R., Filev, D.P.: Summarizing data using a similarity based mountain method. Information Sciences **178**(3) (February 2008) 816–826
21. Zwick, R., Caristein, E., Budescu, D.V.: Measures of Similarity Among Fuzzy Concepts: A Comparative Analysis. International Journal of Approximate Reasoning **1**(2) (April 1987) 221–242
22. Turksen, I., Zhao, Z.: An approximate analogical reasoning approach based on similarity measures. IEEE Transactions on Systems Man and Cybernetics **18**(6) (November 1988) 1049–1056

23. Xuecheng, L.: Entropy, distance measure and similarity measure of fuzzy sets and their relations. Fuzzy Sets and Systems **52**(3) (1992) 305–318
24. Li, Y., Qin, K., He, X.: Some new approaches to constructing similarity measures. Fuzzy Sets and Systems **234**(0) (2014) 46–60
25. Zeng, W., Li, H.: Inclusion measures, similarity measures, and the fuzziness of fuzzy sets and their relations. International Journal of Intelligent Systems **21**(6) (2006) 639–653
26. Dubois, D., Prade, H.: Fuzzy sets and systems: theory and applications. Academic Press, New York (1980)
27. Zhang, B.L., Zhang, H., Ge, S.S.: Face Recognition by Applying Wavelet Subband Representation and Kernel Associative Memory. IEEE Transactions on Neural Networks **15**(1) (January 2004) 166–177
28. Tanaka, G., Aihara, K.: Complex-Valued Multistate Associative Memory With Nonlinear Multilevel Functions for Gray-Level Image Reconstruction. IEEE Transactions on Neural Networks **20**(9) (September 2009) 1463–1473
29. Valle, M.E.: A Robust Subspace Projection Autoassociative Memory Based on the M-Estimation Method. Accepted for publication at IEEE Transaction on Neural Networks and Learning Systems